Chapter 5

Development of a Biomass Gasification integrated Solar –Wind Driven Hybrid System using Organic Rankine Cycle for combined Electricity generation and Hydrogen Production

In this chapter, three configurations, namely, a concentrating solar collector powered pre-heater unit integrated with a conventional biomass gasification system, a Solar ORC system integrated with SOEC (co-electrolysis) and a wind powered variant of the above mentioned systems has been analyzed. This chapter concludes that inclusion of Solar energy reduces the amount of air needed in the gasifier and thus reduces the amount of carbon dioxide produced. The objective of work in this chapter is to study the effect of different operating parameters (gasification temperature, solar irradiance, area of solar collector and water to biomass ratio) along with various performance parameters (production of syngas, methane, hydrogen, total combustible gas, Performance Index) on the three aforementioned configurations simulated via Aspen Plus simulator package.

5.1 Model Layout

Cycle-4. A concentrating solar collector powered pre-heater unit integrated with a conventional biomass gasification system

The proposed model consists of a biomass gasification unit to produce syngas integrated with a parabolic trough solar collector. The gasification unit has been already analyzed in three configurations in previous work. The biomass and water streams enter the gasifier after passing through mixer (M), pump (P) and Pre-heater (Pre-H). After the mixture (biomass + water) enters into the gasifier unit which is made up of two aspen blocks: RYIELD and RGIBBS. Biomass (defined as a non-conventional solid in Aspen Plus) does not have a defined molecular weight and so regarded as a non-conventional mass flow stream. For Aspen Plus to process such a stream, It must be decomposed it into its elementary, conventional components (C, H_2, O_2, N_2, Cl and S) which is done by the help of the RYIELD reactor block. The RGIBBS reactor block employs principle of Gibbs free energy minimization calculations in order to model chemical

equilibrium at a specified temperature and pressure. For isothermal conditions, the excess heat generated in the Gasifier must be removed; this purpose is served by heat stream (Q-2) which takes away net heat output from the RGIBBS reactor. Another heat stream (Q-1) carries the heat of reaction, which has to be given to the RGIBBS to carry out the endothermic gasification reactions, from RYIELD to RGIBBS. In order to decrease Q-2 a pre-heater is utilized to heat the biomass and water mixture before gasifier inlet. The heat in the pre-heater is obtained by the help of a concentrating type parabolic trough solar collector. The layout of this system is shown in Fig.5.1.

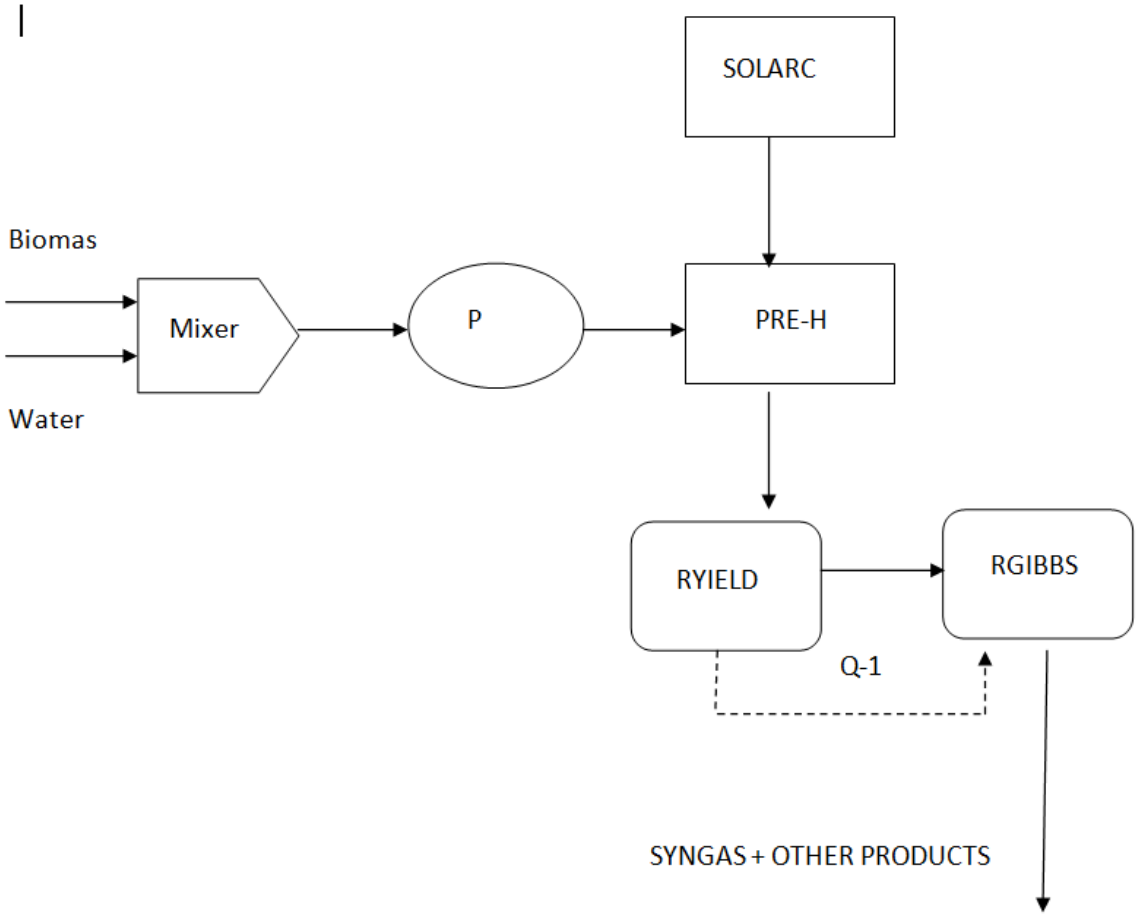

Fig.5.1 Layout of Solar Assisted Gasification System

Cycle-5: A Solar ORC system integrated with SOEC (co-electrolysis) unit

A traditional ORC is combined with a parabolic trough solar collector; where heat in evaporator has been extracted from solar collector. The power generated in the Turbine has been used for Co-electrolysis in a SOEC unit. The layout of this model has been shown in Fig.5.2.

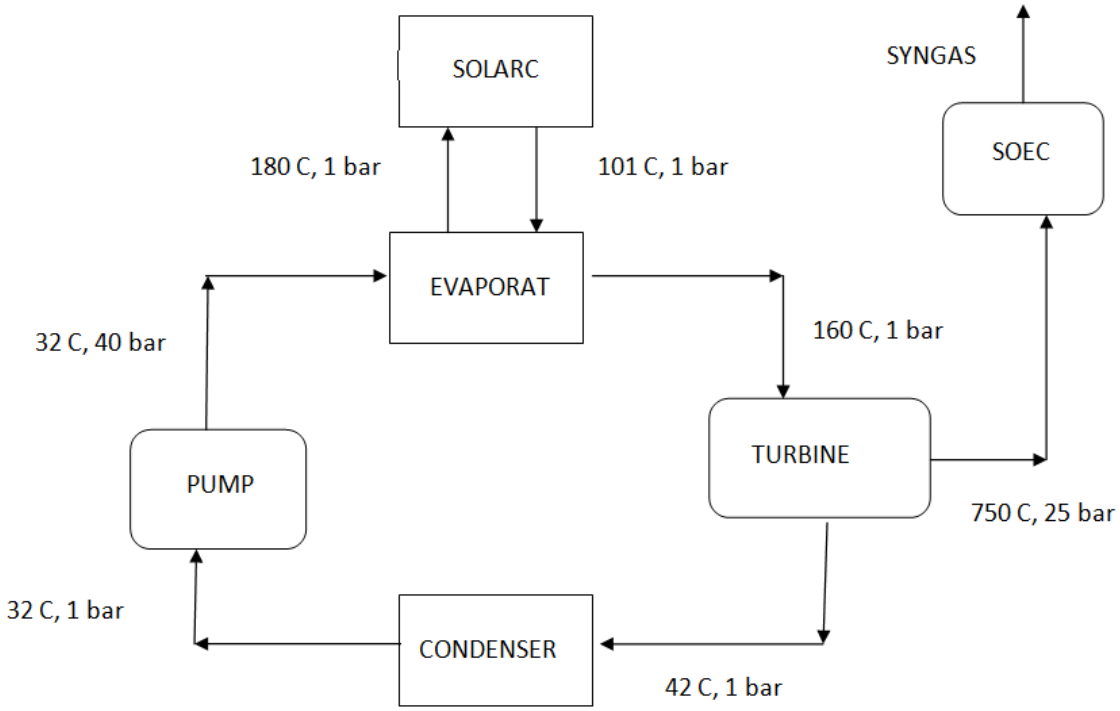

Fig. 5.2 A Solar ORC system integrated with SOEC (co-electrolysis) unit

Co-electrolysis process in the SOEC is commonly modeled considering three consecutive stages: i) the reactant gases come to equilibrium with respect to the water-gas shift reaction, ii) the electrochemical reactions occur in the electrolysis cells, and iii) the produced gases again come into equilibrium according to reactions 4 and 5 before exiting the cathode compartment. The Reactions which takes in the SOEC have been shown in Table.1.

No	Reaction	Heat of Reaction (kJ/mol)
1	$H_2O + 2e^- \rightarrow H_2 + O^{2-}$	+241.8
2	$CO_2 + 2e^- \rightarrow CO + O^{2-}$	+393.5
3	$2O^{2-} \rightarrow 2O_2 + 4e^-$	---
4	$CO + H_2O \rightleftharpoons H_2 + CO_2$	-41
5	$CO + 3H_2 \rightarrow CH_4 + H_2O$	-206.1
6	$CO + H_2 \rightarrow C(S) + H_2O$	-131.3
7	$2CO \rightarrow C(S) + CO_2$	-172.5

Table.5.1. Main reactions in Solid oxide electrolyser

There is no single component in ASPEN Plus standard library to model the SOEC, hence three separate reactors are used to take these individual stages (occurring simultaneously) into account (Fig.3). In the first reactor (PRE-WGSR), the reactants (S13) will reach equilibrium based on reaction 4. Then this equilibrium mixture (S23) will go through the electrochemical reactions in the second reactor (SOEC) which results in production of syngas and oxygen. In reality, oxygen and syngas are produced separately in cathode and anode compartments, respectively. To take this fact into account, the exhaust from second reactor (S24) passes through a separator where oxygen content of stream is separated (S26) from the remainder (S25). In the third and last reactor (POST-WGS), the gas mixture (S25) will reach the equilibrium based on the water gas shift and methanation reactions (reactions 4 and 5) [18,58]. The Gibbs reactor (RGibbs) is used to model the first and third reactors whereas stoichiometry reactor (RStoic) is selected for the second reactor.

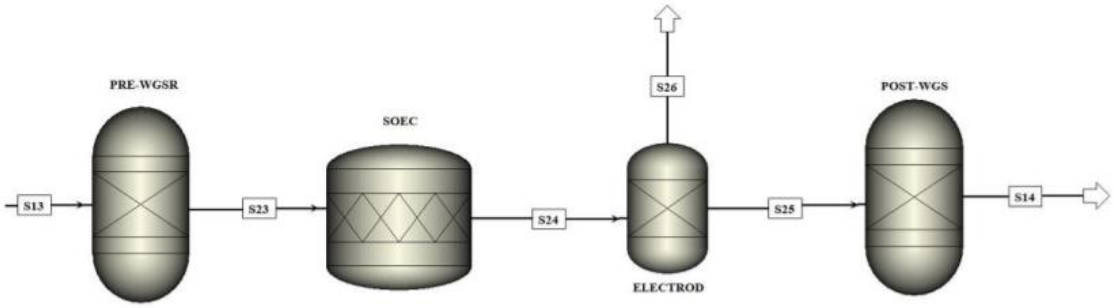

Fig.5.3 SOEC model layout in Aspen Plus

Cycle-6a: Wind and Solar Powered Biomass Gasification System

The configuration of this cycle is similar to Cycle-4 but with one major difference; a wind turbine has been used to supply electric power to the system.

Cycle-6b: Wind and Solar Powered ORC system integrated with SOEC (co-electrolysis) unit

In this also a wind turbine has been used to supply power to the system. The rest of the configuration of this cycle is congruent to Cycle-5.

5.2 Mathematical Model

The analysis of proposed cycles has been based on the energy balance of each component. For the modeling of the proposed system the following assumptions have been considered:

1. Steady state has been achieved and the heat exchanges with the surroundings are neglected.
2. Reaction of sulfur has not been considered in the gasification model.
3. Devolatilization of biomass happens instantaneously and volatile products mainly consist of H_2O, H_2, CO, CO_2, CH_4, C_2H_6, N_2, NO_2, NO, NH_3 and O_2.
4. Catalytic effect of char has not been considered in the model.
5. Sufficient amount of cooling water has been assumed to be available and sink temperature for the model has been taken as 30^oC.
6. Turbine and pump have isentropic efficiencies to include losses.

7. In all the heat exchangers, heat transfer takes place under isobaric conditions.
8. Heat exchanger modeling has been done by pinch point temperature approach.
9. The Aspen User subroutines for Solar and wind have efficiencies accounted to model the irreversibilities.
10. Global solar irradiation is assumed to be composed only of Direct and Diffuse radiations.
11. Solar Concentrating Factor was taken to be 50.

The reversible voltage of electrolysis cells, also known as Nernst voltage, depends on the operating temperature of electrolyser and partial pressures of the reactants. Nernst voltage, V_N, at the given operating condition in case of co-electrolysis is reported as the weighted average of steam and carbon dioxide reversible voltage values as shown in equation 5.1,

$$V_{N,Co-electrolysis} = \frac{1}{y_{H_2o} + y_{Co2}} \left\{ \begin{array}{l} y_{H_2o}\left(\frac{-\Delta G_{f,H2O(T)}}{2F} - \frac{RT}{2F} \ln\left[\left(\frac{y_{H_2o}}{y_{H_2}.y_{o_2}^{0.5}} \right) \left(\frac{P}{P_{std}} \right)^{-0.5} \right] \right) \\ + y_{CO2}\left(\frac{-\Delta G_{f,CO2(T)}}{2F} - \frac{RT}{2F} \ln\left[\left(\frac{y_{CO2}}{y_{CO}.y_{o_2}^{0.5}} \right) \left(\frac{P}{P_{std}} \right)^{-0.5} \right] \right) \end{array} \right\} \quad (5.1)$$

$\Delta G_{f,H2O(T)}$ and $\Delta G_{f,CO2(T)}$ represent the Gibbs free energy of formation at SOEC operating temperature of steam and carbon dioxide respectively, y_i is the molar fraction of each component in the stream, P is the electrolyser pressure, T is the operating temperature and F is the Faraday constant.

The total loss mechanism in the operating cell is normally defined as area-specific resistance (ASR) which is assumed to follow an Arrhenius relationship to temperature (Becker et al., 2012, Stoots et al., 2009):

$$ASR(T) = ASR_{1100K} - 0.463 + 3.973 * 10^{-5} \exp\left(\frac{10300}{T}\right) \quad (5.2)$$

The effect of operating pressure, however, is not considered in this equation. To include the effect of pressure in the model, ASR is calculated using the experimental relationship to operating temperature and pressure (Giglio et al., 2015):

$$ASR(P,T) = \left\{ \begin{array}{ll} 34.22e^{-0.0054T}e^{-0.0271P} & co-electrolysis \\ 35.51e^{-0.0058T}e^{-0.0271P} & steam-electrolysis \end{array} \right\} \quad (5.3)$$

The operating voltage of the electrolysis cells at the operating condition can be estimated based on the values of V_N, ASR, and current density, i.

$$V_o = V_N + ASR(T).i \tag{5.4}$$

Current density is a design choice and normally is selected to be equal or close to the thermo-neutral current density of the electrolysis process at the given condition [Sun et al., 2012]. This is the point of operation where the supplied electricity is in the range of the thermal energy of endothermic electrochemical reactions (Bierschenk et al., 2011). In other words, the electrolyser neither requires nor releases heat. Hence, thermal management of SOEC would be less complex. A heat source would be necessary in cases that the electrolyser operates below this point, otherwise SOEC temperature will drop uncontrollably. On the other hand, not only heat management would be crucial when SOEC operates above thermo-neutral point but also electrolysis unit performance declines (Sun et al., 2012, Bierschenk et al., 2011, Graves et al., 2011). Thermo-neutral current density can be estimated as (Giglio et al., 2015),

$$i_{TN} = \frac{V_{TN} - V_N}{ASR} = \frac{T\Delta S}{2F.ASR} \tag{5.5}$$

Where ΔS is the entropy change of reactants taking part in the electrochemical reactions.

Table 5.1 shows the calculated values of open circuit voltage and area specific resistance from the theoretical model. To validate the model results, these values are compared to the measured values from the experiments done by Ebbesen et al., 2009 and Jensen et al., 2010. In the former case, the experimental values are presented for the thermodynamic equilibrium composition of the mixture at each temperature. In the latter, to be in agreement with the experimental conditions, the temperature is kept constant at 750 ^{o}C and stream composition was assumed to be comprised of 50% H_2 and 50% H_2O while pressure varied. As can be seen, the calculated values are quite comparable to the experimental ones, therefore the developed model is judged to fairly represent behavior of solid oxide electrolyser units.

Table 5.1 Comparison between the calculated open circuit voltage and area specific resistance with the measured values presented by Ebbesen et al., 2009 and Jensen et al., 2007.

Operating Condition	Area Specific Resistance(Ω/cm^2		Open circuit voltage (V)	
Temperature(^oC)	Model	Experiment	Model	Experiment
Co-electrolysis				
750	0.38528	0.51	0.952872	0.843
800	0.288291	0.37	1.001895	0.869
850	0.215717	0.26	1.025999	0.89
R^2	0.99			0.98
Steam-Electrolysis				
750	0.50118	0.41	0.943569	0.982
800	0.382591	0.27	0.935902	0.967
850	0.292062	0.19	0.922562	0.951
R^2	0.99			0.98
Pressure (bar)				
0.4	0.45436	0.59	0.888409	0.961
1	0.448482	0.52	0.904604	0.969
3	0.429435	0.47	0.925979	0.996
10	0.368916	0.42	0.946467	1.011
R^2	0.77			0.97

5.3 Results and Discussion

The investigation of the proposed model have been carried out for two water to biomass ratios (0.4 and 0.6), three solar collector areas (10 m^2, 20 $m^2$and 30 m^2), different Sunlight hours (8 am to 4 pm denoted by corresponding numbers 1-9), various gasification temperatures (500K-1400K) and two biomass materials namely, PMSC and LW (see Table 4.2). Different configurations were analyzed separately under different conditions. Firstly, the temperature of gasification has been optimized for each of the biomass materials and WBR under consideration. This has been mentioned in section 4.3 of this thesis. This section also describes the effect of WBR on syngas and hydrogen production. Secondly, output parameters of each cycle have been analyzed.

Effect of Gasification temperature, Sunlight hours and Collector area on Output Parameters of Cycle-4

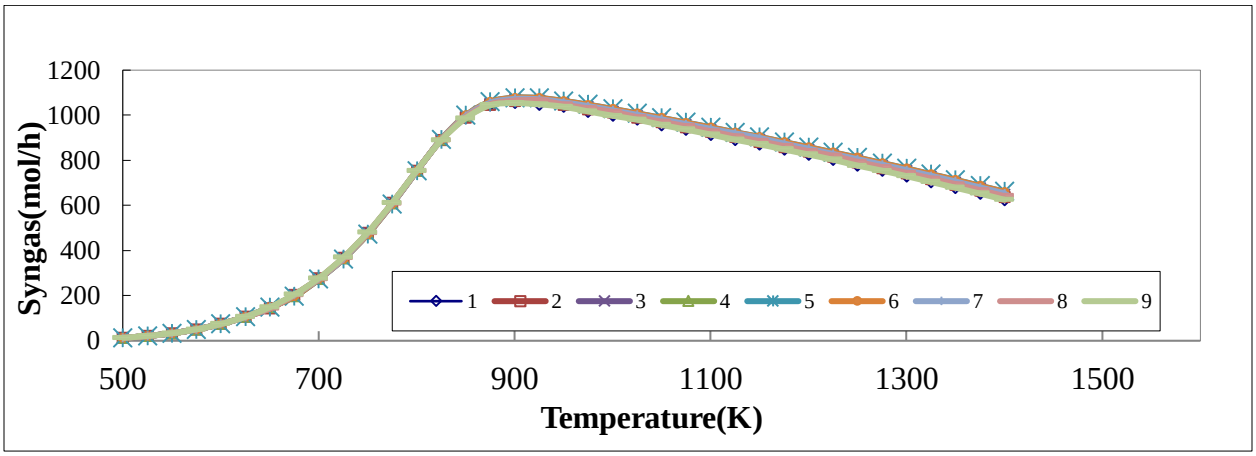

Fig. 5.4 Variations of syngas with gasification temperature for PMSC at constant collector area (=10 m^2) but with varying Sunlight hours

Fig.5.4 shows the variation of Syngas with gasification temperature at different sunlight hours for constant collector area (10 m^2). It must be reported that for a constant sunlight hour the syngas production increases with increase in gasification temperature but after reaching a maxima it starts to decrease. The syngas production below the gasification temperature,

corresponding to maximum syngas production, was constant for all the sunlight hours whereas above this gasification temperature the syngas production first increases and then decreases as sunlight hours increases. The hydrogen Production (fig. 5.5) also shows a similar trend but with steeper plot curve after maxima has been reached.

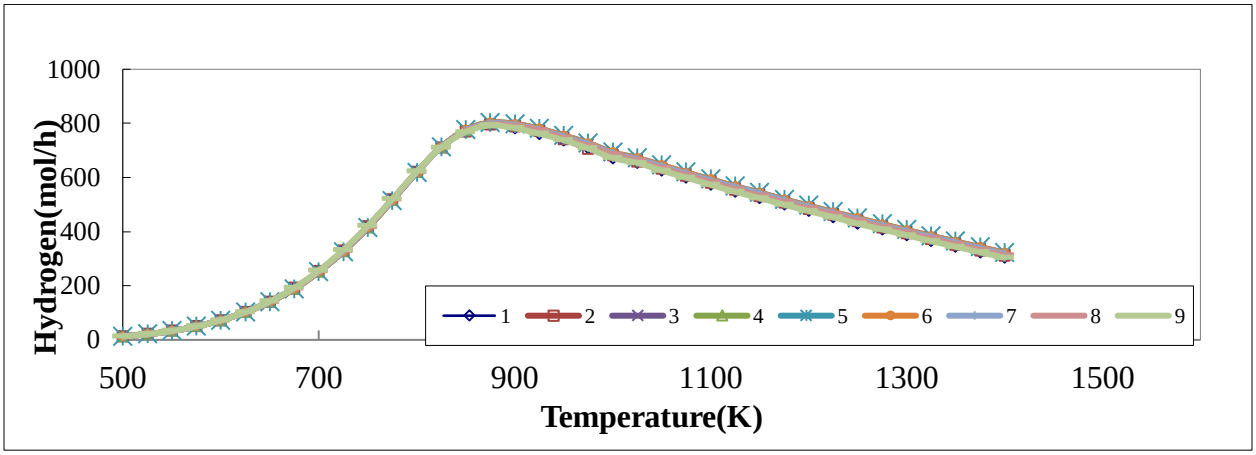

Fig. 5.5 Variations of Hydrogen gas with gasification temperature for PMSC at constant collector area (=10 m^2) but with varying Sunlight hours

The Air required in the Gasifier unit as shown in Fig. 5.6 increases with increase in gasification temperature but decreases with increase in sunlight hours. There is a minor hump in the plot which shows an increase in Air requirement in a particular range of gasification temperatures. It must also be reported that at gasification temperatures lower than 700K the value of Air required is negligible as the heat of reactions is already positive or reactions are exothermic and not endothermic.

Fig.5.7 shows variation Syngas with gasification temperature at a fixed sunlight hour (=12 pm) but with varying collector area. It can easily be observed that syngas production first increases upto a maximum value and then decreases. However, for higher collector area more syngas is generated than at lower collector area. A similar trend is also observed in Carbon dioxide formation but at lower values of collector area more carbon dioxide is produced than at higher values (Fig. 5.8).

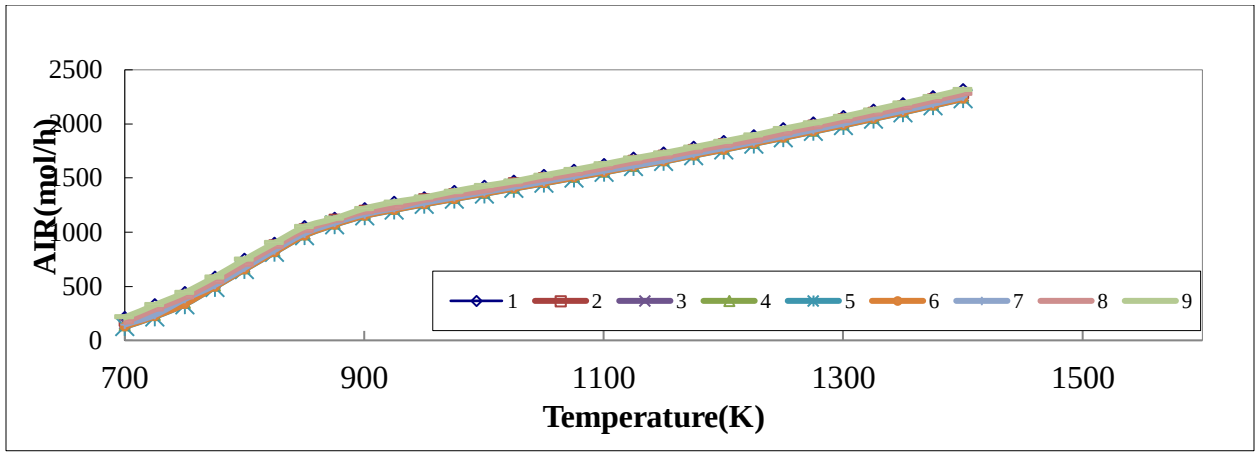

Fig. 5.6 Variations of Air required in the gasifier with gasification temperature for PMSC at constant collector area (=10 m^2) but with varying Sunlight hours

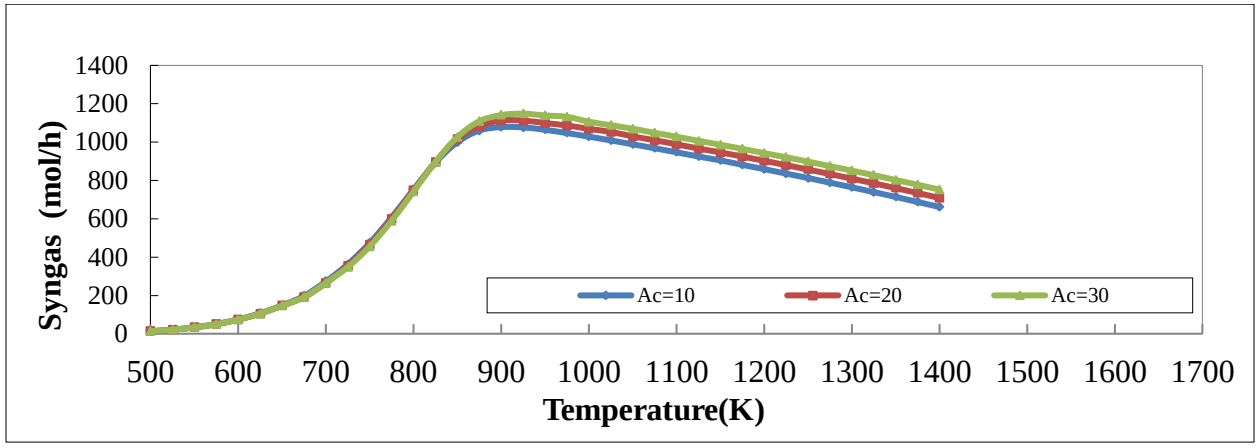

Fig. 5.7 Variations of syngas with gasification temperature for PMSC at constant sunlight hour (=12 pm) but with varying collector area

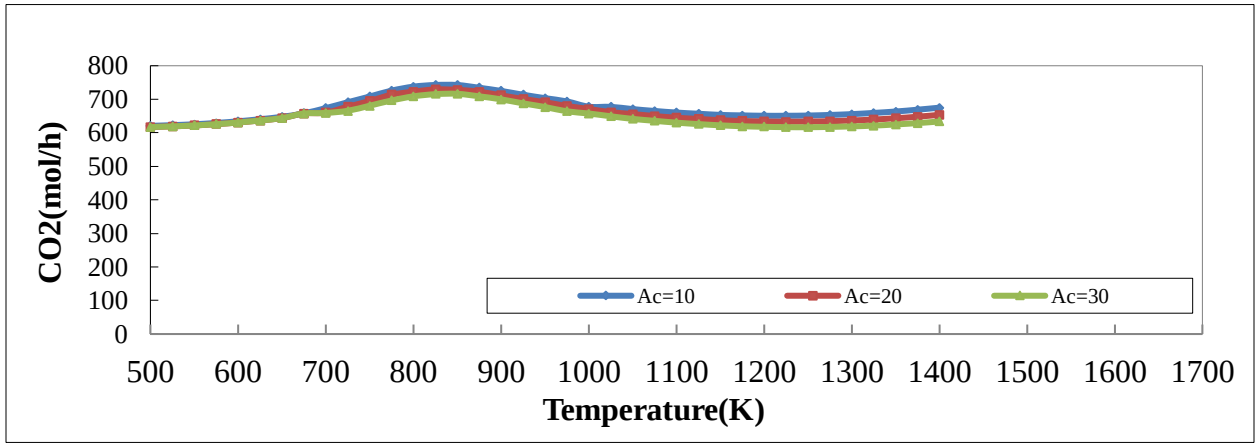

Fig. 5.8 Variations of Carbon dioxide with gasification temperature for PMSC at constant sunlight hour (=12 pm) but with varying collector area

Another approach has been adopted where gasification temperature is kept constant and sunlight hours have been varied (Figs.5.9-5.13). As shown in Fig. 5.9, Syngas formation first increases as solar intensity increases in the solar collector upto a maximum value and then decreases as solar irradiation decreases. The amount of syngas generated is higher for lower values of gasification temperature except for 800K. A similar trend is also observed for hydrogen gas (Fig.5.10). However, it must be noted that Syngas production at gasification temperature of 800K is almost constant and hydrogen production at gasification temperature of 800K show unprecedented results. Carbon dioxide generation is found to decrease as the solar intensity increases and then increases after attaining a minimum value (Fig. 5.11). Higher values of gasification temperatures produce lower carbon dioxide.

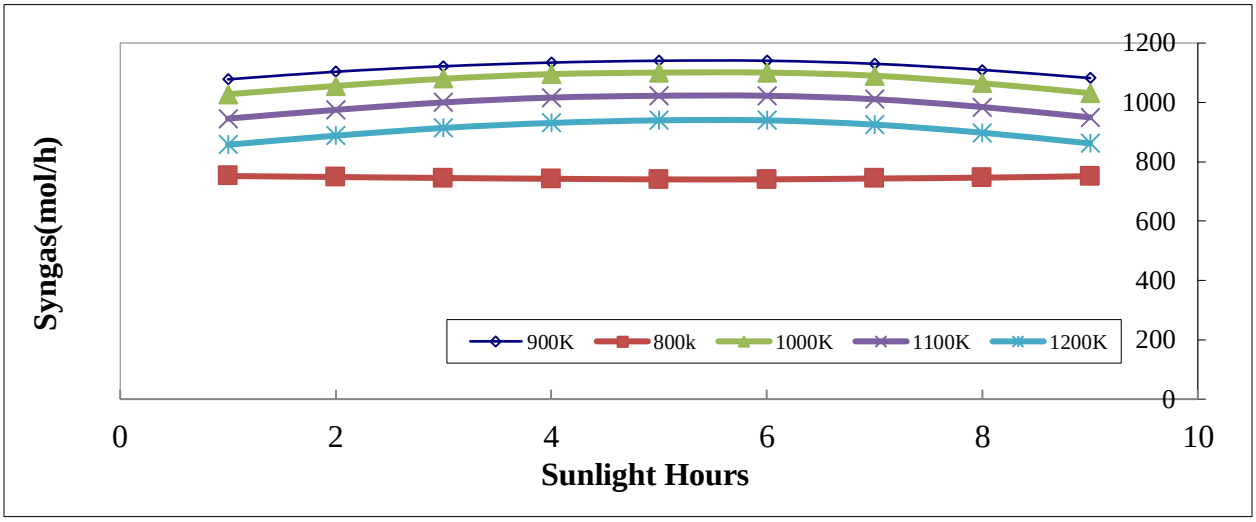

Fig. 5.9 Variations of Syngas with Sunlight hours for PMSC at constant collector area (=30 m^2) but with varying Gasification Temperature

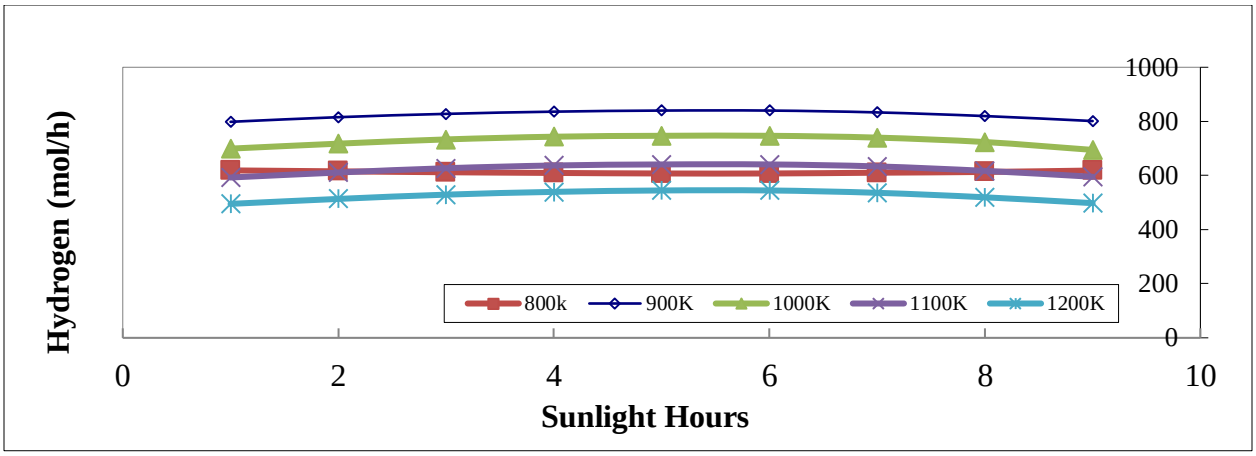

Fig. 5.10 Variations of Hydrogen with Sunlight hours for PMSC at constant collector area (=30 m^2) but with varying Gasification Temperature

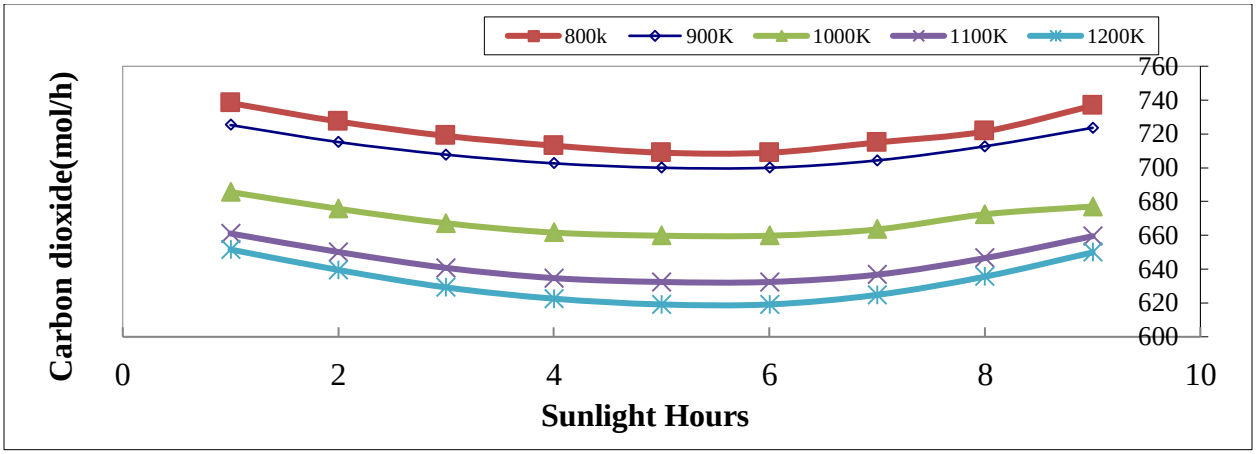

Fig. 5.11 Variations of Carbon Dioxide with Sunlight hours for PMSC at constant collector area (=30 m^2) but with varying Gasification Temperature.

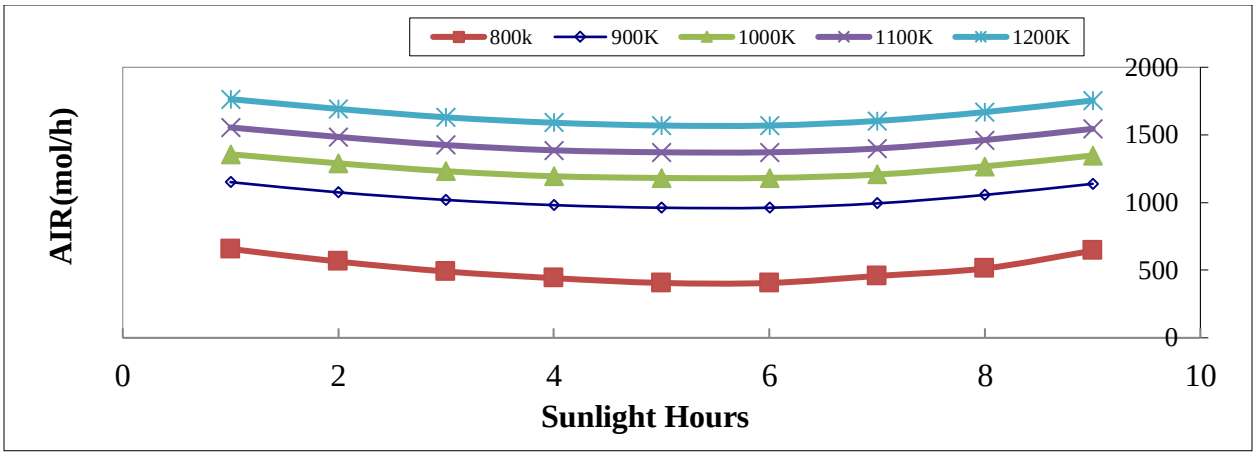

Fig. 5.12 Variations of Air required in the gasifier with Sunlight hours for PMSC at constant collector area (=30 m^2) but with varying Gasification Temperature

The Air required in the gasifier as shown in Fig. 5.12, illustrates a boat shaped curve similar to Carbon dioxide. The amount air inlet into the gasifier is found to be directly proportional to the gasification temperature i.e. lower temperatures require less air into the gasifier. Fig.5.13 presents behaviour of Air required in the gasifier with solar collector and without solar collector. The trend observed is similar as above but with a noted difference that air requirement is significantly reduced in the case of preheating. Thus, the amount of Carbon dioxide produced also decreases.

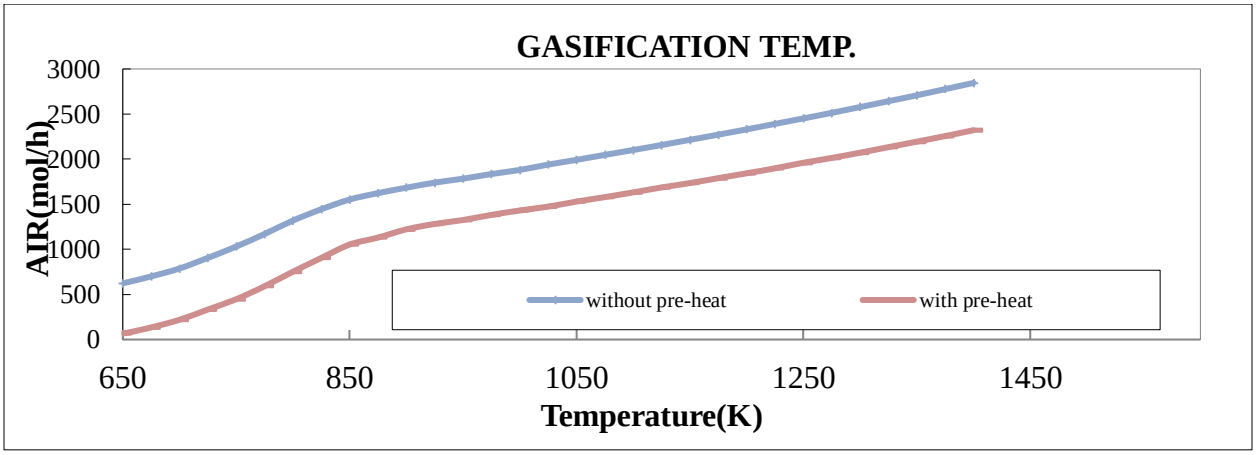

5.13 Plot of Air required in the Gasifier with and without solar collector (or Pre-heat) vs Gasification Temperature

Effect of Sunlight hours and Collector area on Output Parameters of Cycle-5

Fig. 5.14 shows the variation of all the product gases of the SOEC with sunlight hours. It can be easily seen that H_2, CO and Syngas first increases and then decreases whereas CO_2 first decreases and then increases as sunlight hours increases. However, in Fig.5.15 Mole fraction of H_2, CO and CO_2 were shown. Hydrogen and Carbon dioxide show similar trend of first decreasing and then increasing after attaining a minimum value whereas CO first increases and then decreases.

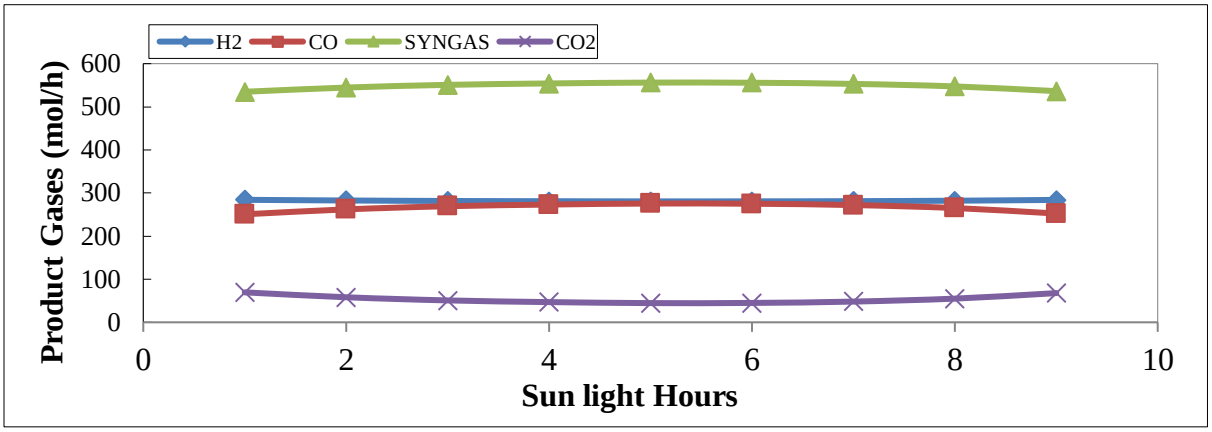

Fig. 5.14 Variation of the product gases of the SOEC with sunlight hours at constant Collector area (=30 m^2)

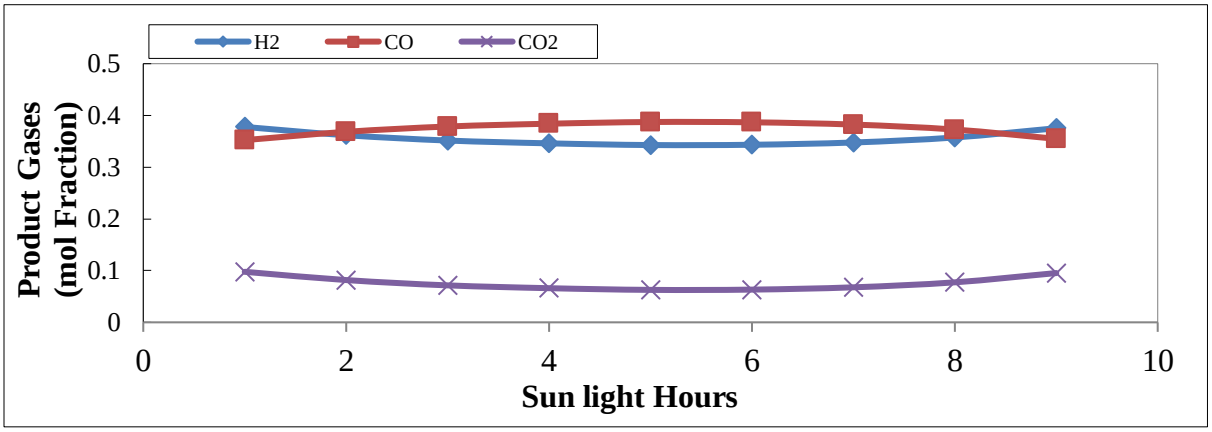

Fig. 5.15 Variation of Mole Fraction of the product gases of the SOEC with sunlight hours at constant Collector area (=30 m^2)

As Depicted in Fig. 5.16, Syngas formation increases upto a maximum value and then decreases as sunlight hours increases. Syngas produced was found to be inversely proportional to the collector area. Furthermore, Hydrogen generation first decreases upto a minimum value and then increases as sunlight hour increases (Fig. 5.17). Also, hydrogen produced was found to be inversely proportional to the collector area similar to syngas. A similar behaviour was also seen for the carbon dioxide as presented in Fig.5.18.

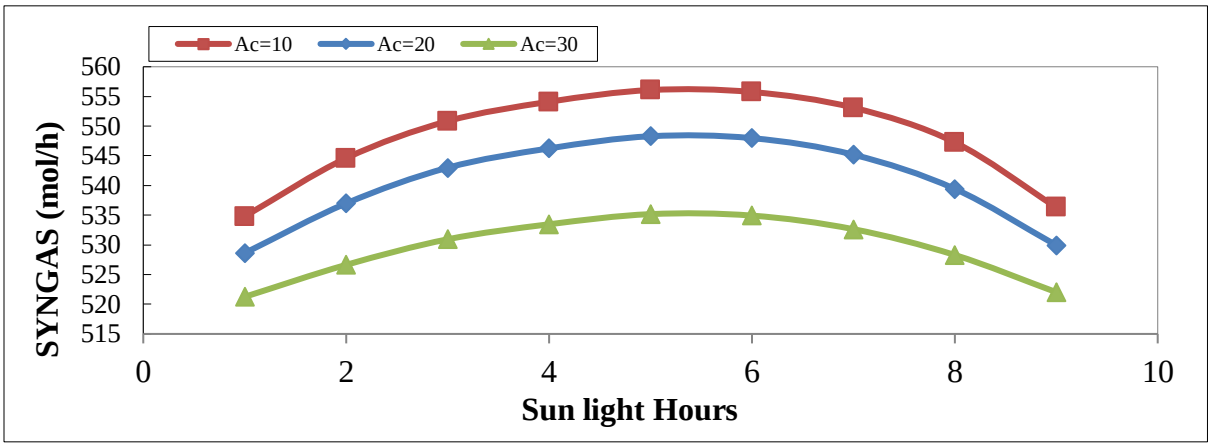

Fig. 5.16 Variation of the Syngas produced from SOEC with sunlight hours at varying Collector area

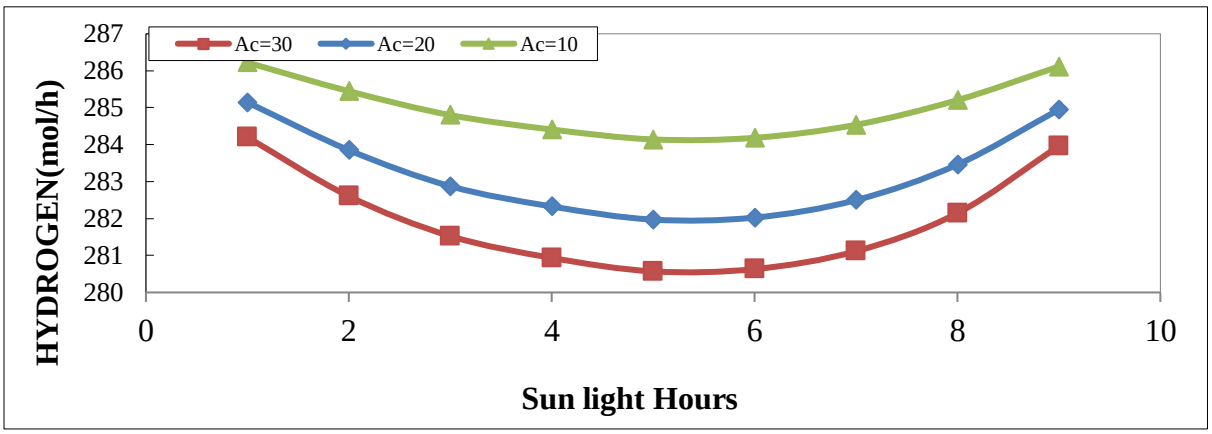

Fig. 5.17 Variation of the Hydrogen produced from SOEC with sunlight hours at varying Collector area

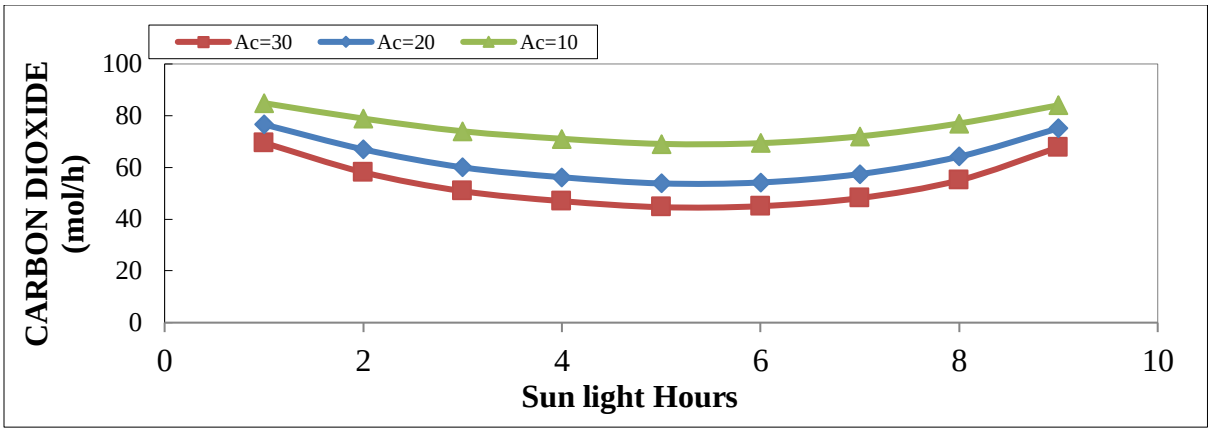

Fig. 5.18 Variation of the Carbon Dioxide produced from SOEC with sunlight hours at varying Collector area

Comparison Performance Index of Cycle-4 and Cycle-5 with Cycle-6a and Cycle-6b

As illustrated in Fig. 5.19, Performance Index of Cycle-4 and Cycle-5 can be easily interpreted. Cycle -5 has been reported to have a higher performance Index (PI) as compared to Cycle-4. Since Cycle-6a and Cycle-6b have wind turbine connected to them to supply much needed electrical power. Therefore, there Performance Index can be calculated by adding this power to the net heat output of the system. The PI of cycle-6a and cycle-6b has been shown in Fig. 5.20. It can be easily concluded that PI for Cycle 6a and Cycle-6b is higher than Cycle-4 and Cycle-5.

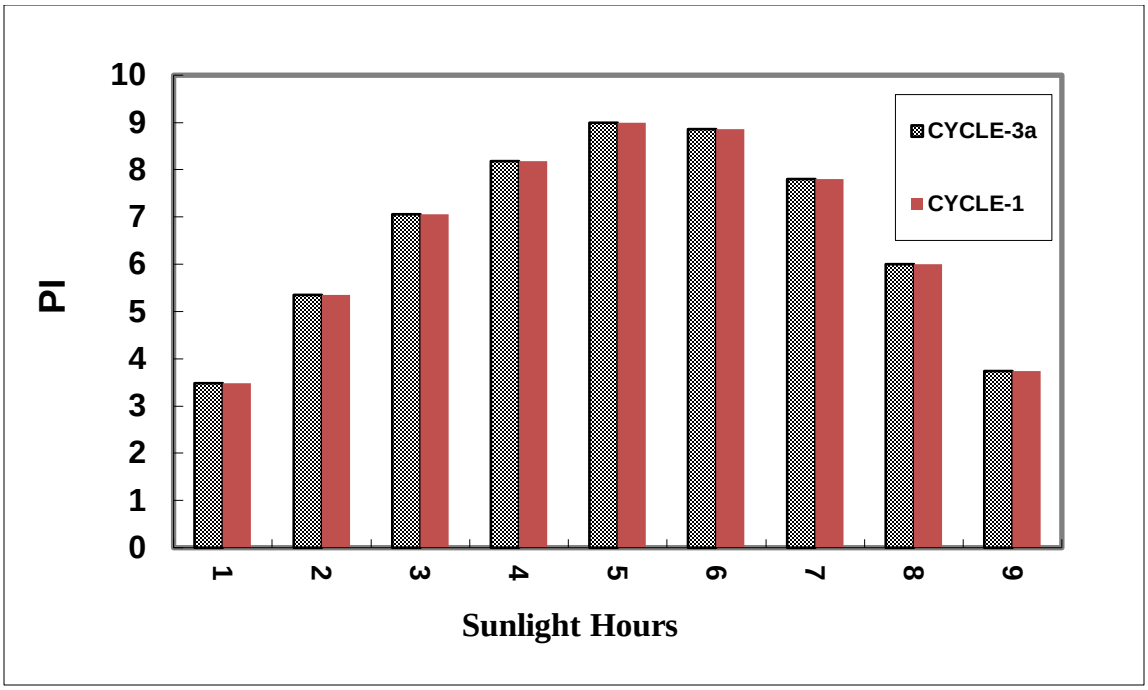

Fig. 5.19 Variation of the Performance Index with sunlight hours at constant Collector area (=30 m^2) and fixed optimum gasification temperature for Cycle-4 and Cycle-6a

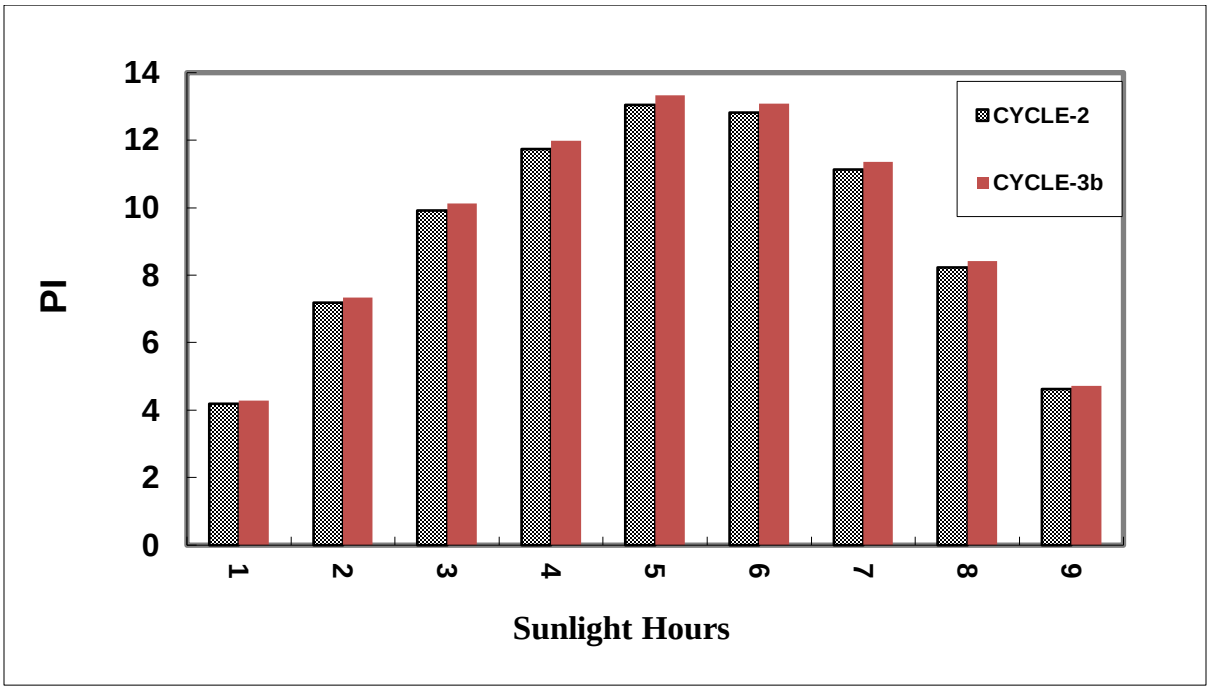

Fig. 5.20 Variation of the Performance Index with sunlight hours at constant Collector area (=30 m^2) and fixed optimum gasification temperature for Cycle-5 and Cycle-6b